DOI: 10.1002/ejic.200601211

Tungsten Oxide and Tungsten Oxide-Titania Thin Films Prepared by Aerosol-Assisted Deposition – Use of Preformed Solid Nanoparticles

Uzma Qureshi,[a] Christopher Blackman,[a] Geoffrey Hyett,[a] and Ivan P. Parkin*[a]

Keywords: Tungsten oxide / Aerosol-assisted CVD / Thin films

Aerosol-assisted deposition (AAD) was used to deposit films of WO_3 from a suspension of solid nanoparticulate WO_3 in toluene. Titania films were deposited by the aerosol-assisted chemical vapour deposition of $[Ti(OiPr)_4]$ in the presence of WO_3 nanoparticles. The WO_3 and TiO_2 films exhibited photoactivity and photoinduced superhydrophilicity, further the titania films showed very unusual highly crenulated microstructures. These microstructures could not be obtained by sol-gel, atmospheric pressure chemical vapour deposition or evaporation routes. Furthermore, the microstructures could not be obtained from $[Ti(OiPr)_4]$ in the absence of nanoparticulate WO_3.

Introduction

Nanoparticles are a major research interest worldwide, and a variety of different shapes and compositions can now be produced.[1,2] Many potential applications depend on formation of a nanocomposite, which serves both to immobilise the particles and render them chemically inert. In addition, the incorporation of nanoparticles into a matrix can change the properties of both the particle and the host. One area that has gained rapid attention is the growth of nanoparticles within a host film.[3–10] The presence of nanoparticles can assist in photogenerated charge separation, and this has been exploited in improved titania photocatalysts,[3,11,12] iron oxide photoanodes,[13] and tungsten oxide photochromic and electrochromic films,[14,15] all with incorporated gold nanoparticles.

Several strategies for production of nanoparticles within a host matrix have been devised including; synthesis of the semiconductor matrix followed by addition of pre-formed nanoparticles in a second step.[3,14–16] synthesis of the semiconductor matrix followed by application of metal ions in a second step; high energy ion implantation[6,17,18] and spin coating with a solution of metal ions followed by photocatalytic reduction or heat treatment[8,19] and synthesis of the semiconductor matrix and metal particles in a single step.[13,20,21] In all of these routes the nanoparticle is either used in a charged charge-stabilised or ligand-stabilised form dissolved in solution or generated in situ.[22] Furthermore, the use of a bulk nanoparticulate powder in forming thin films has not been investigated.

The physical state and composition of a precursor are critical in determining the quality of a thin film. In both physical vapour deposition (PVD) and chemical vapour deposition the precursor is transported through a vacuum or gas medium in the form of reactive atoms or molecular entities. These then undergo various surface reactions to form the desired film. The precursors are typically metal or ceramic tablets in the case of PVD, or volatile molecular entities in the case of CVD. On occasions the CVD process has been modified so that molecular precursors that are involatile or that undergo too ready a decomposition are first dissolved in an aerosol, and the aerosol is used as the transport medium to deliver the precursor to the substrate surface. Much work in this area has been pioneered by O'Brien.[23] Preformed bulk solids, suspended in a solution, have not been used in aerosol-assisted chemical vapour deposition. The use of solid particles to form thin films is however well known in a number of processes, in particular cold-spraying, plasma-spraying and thermal-spraying.[24] In these techniques either the solid particles are fired at very high kinetic energies at the surface, normally by a plasma-jet and a coating is formed by "splatting" of the solid on the surface or hybrid thermal-spraying is used in which some movement or reaction of the particles occurs on the surface.[24–26] One very new and emerging area of spraying technology is the use of suspension plasma spraying (SPS), using d.c. or R.F. plasma spray torches, in which powder particles are injected into the plasma flow using a liquid as carrier media, instead of the classical carrier gas.[26] This new approach offers unique possibilities to carry nanosized particles to manufacture finely grained coatings.

This paper details the preparation of WO_3 thin films from preformed commercially available solid nanoparticulate WO_3 using aerosol-assisted transport. These solid nanoparticles were used in a conventional CVD experiment using an aerosol as a carrier medium. Parallels to spray coating exist except that a high velocity gas stream or reactive plasma was not required. A separate set of experiments

[a] Department of Chemistry, University College London, 20 Gordon Street, London, WC1H OAJ, UK

investigated what happened when the WO_3 nanoparticles were added to a titanium dioxide AACVD precursor, which was then used to deposit thin films with small tungsten contents but greatly ordered titania microstructures. This work shows that solid nanoparticles can be used and transformed into an adhesive thin film provided that they can be dissolved/suspended in an appropriate carrier solvent and without the use of plasma spraying or high velocity "splatting". Furthermore, these nanoparticulates may act as templates to influence the production of highly unusual microstructures from traditional CVD precursors.

Results and Discussion

Preparation of WO_3 Thin Films by Aerosol Transport from Solid Nanoparticulate WO_3

Tungsten oxide thin films were prepared on glass from the aerosol-assisted deposition (AAD) of commercial nanoparticulate tungsten oxide powder. The films were uniform and pale yellow in colour. They covered the glass substrate. The films passed the Scotch tape test, were adhesive, could not be wiped off but could be scratched with both a brass and steel stylus. Interestingly all of the deposition was on the top substrate plate rather than the heated bottom plate (even with lower substrate temperatures). We have prepared tungsten oxide films by conventional atmospheric pressure chemical vapour deposition, film formation is then on the heated substrate. The films formed previously by conventional APCVD or reported here by aerosol-assisted AAD show similar properties except that by conventional CVD formation of substochiometric WO_{3-x} is an issue.[18]

X-ray powder diffraction of the tungsten oxide films showed that the material was crystalline (Figure 1) with the fully stoichiometric triclinic WO_3 structure. This matched exactly by eye the diffraction pattern of the initial powder although perhaps some slight grain growth occurred. The indexed cell constants (from Reitveld analysis[29]) for the starting nanoparticulate powder were a = 7.285(1) Å, b = 7.488(1) Å, c = 7.650(1) Å; α = 89.57(3)°, β = 90.18(4)°, γ = 90.81(1)° and for the thin film a = 7.321(1) Å, b = 7.525(1) Å, c = 7.683(2) Å; α = 89.58(3)°, β = 90.18(1)°, γ = 90.78(1)°. These cell constants compare very favourably with those obtained on triclinic WO_3 by Woodward et. al.[20] a = 7.312(1) Å, b = 7.525(1) Å, c = 7.689(1) Å; α = 88.847(3)°, β = 90.192(4)°, γ = 90.94(1)°. The X-ray pattern of the thin film indicates that there is no significant preferred orientation of the crystallites on the surface. This is completely different to conventional atmospheric pressure CVD and aerosol-assisted CVD approaches to tungsten oxide on glass where preferred orientation in the (020) direction predominated.[28] Average crystallite sizes as determined by XRD line broadening using the Scherrer equation (GSAS) were 199(2) Å for the starting powder as and 227(2) Å for the thin film.[29] This indicates some slight grain growth or selective deposition of the slightly larger grains within the weighted average crystallite size.

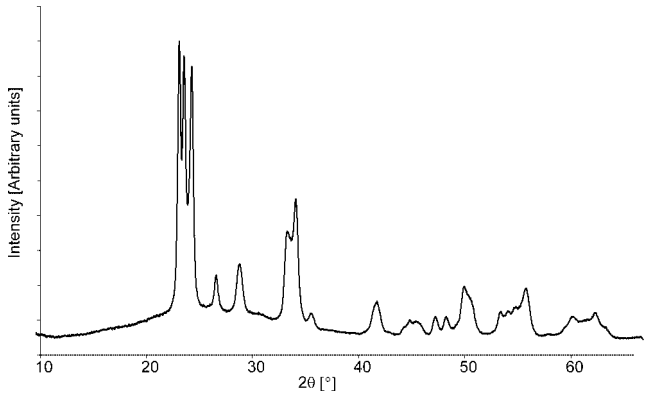

Figure 1. X-ray powder diffraction pattern of the WO_3 films formed at 450 °C by the aerosol-assisted deposition of nanoparticulate WO_3 suspended in toluene.

Scanning electron microscopy of the tungsten oxide thin films showed a dense continuous film made up of interlocking particles of approximate size 20–50 nm, Figure 2. EDX analysis showed that the films contained only tungsten and oxygen in a 1:3 ratio. The initial tungsten oxide powder was examined by TEM before the aerosol-assisted process. The powder was made up of agglomerates, however a number of small isolated WO_3 particles of size 15–20 nm could be seen. The Raman pattern for the as formed WO_3 film is identical to the starting material and is a perfect match for triclinic WO_3.[21]

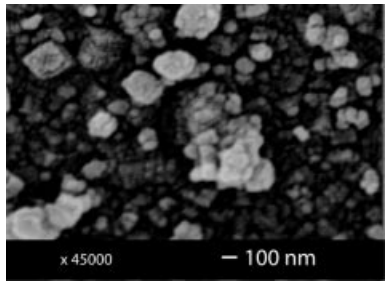

Figure 2. Scanning electron micrograph of the WO_3 films formed at 450 °C by the aerosol-assisted deposition of nanoparticulate WO_3 suspended in toluene.

The tungsten oxide films displayed two useful functional properties – they were active photocatalysts and they showed photoinduced superhydrophilicity. The contact angle for water droplets on the tungsten oxide thin films was very low – between 3–7°, indicating that the surface is very hydrophilic. This contact angle dropped further to between 0.5–2° on exposure of the surface for 0.5 h to 254-nm radiation. On keeping the samples in the dark for 24 h the contact angle increased to 7–8°, and on further irradiation decreased again to between 0.5–2°. The reversible change in contact angle with light/dark storage has been observed before for TiO_2 films.[31] The explanation was that in the light Ti^{III} hydroxide centres are created at the surface which strongly hydrogen bond water and hence reduce the contact angle. A slower oxidative process reverts the Ti^{III} to Ti^{IV} with release of water and loss of the hydroxy groups. In the dark formation of Ti^{IV} predominates as there is no light to

promote Ti^{III} formation, and the films become less hydrophilic. The same behaviour could be responsible for what is seen for the tungsten oxide films with formation of a hydroxylated surface in the light and its subsequent loss on oxidation in the dark. A slight colour change was noted between the films kept in the dark which were pale yellow, and those exposed to light which were slightly darker, this could indicate some W^{V} centre formation. The observed water contact angles of the WO_3 films are lower – that is the films are more hydrophilic than WO_3 made by APCVD and AACVD using traditional soluble molecular precursors.[32] This change in contact angle with time was repeated over many light-dark cycles. The very low initial contact angle puts these films in the class of superhydrophilic films and gives lower measurements to that of titanium dioxide thin films formed from sol-gel or CVD. The contact angle is probably a consequence of the surface being both partially hydroxylated and hence able to hydrogen bond effectively to the water, and having high porosity engendered by having a very fine microstructural form of nanoscaled particles. The WO_3 films readily destroyed a stearic acid overlayer and did so with both 254 and 365 nm irradiation, rates of destruction (1.5×10^{12} molecules $cm^{-2}min^{-1}$ for 254 nm) were similar to previously reported CVD prepared WO_3 and TiO_2 thin films.[30,32,33]

The aerosol transport method provides a ready means of forming thin films from a solid and completely involatile precursor. The fact that the initial tungsten oxide powder was made of nanoparticles probably helped suspension into the toluene solution and facilitated transport of the nanoparticulate solid to the substrate where the aerosol evaporated; and a thin film was laid down on the upper substrate. Notably the initial nanoparticle crystallite sizes (15–20 nm) are considerably smaller than the aerosol droplets (20 μm). The films formed, however, did seem to be composed of nanoparticulates as judged by SEM, although some agglomeration was noted. There seems to have been some sintering and partial crystal growth during the aerosol-assisted transport and deposition. Notably the large agglomerates (micron sized) that were observed in the initial starting powder were not seen in the thin films. Furthermore, these agglomerates did not dissolve in the initial precursor solution and were not found in the reactor flask after the deposition. Some evidence of larger agglomerates was seen in the exhaust of the reactor. Hence in this system we believe that the initial powder gets effectively transferred in the aerosol process. The film that is formed is on the top plate of the reactor and is composed of only relatively small nanoparticulates that are interlocked together – rather than the agglomerated particles seen by TEM in the initial starting powder. The best explanation for this is the thermophoretic effect. Large particles can not diffuse through the stagnant boundary layer effectively due to a buoyancy effect where faster moving gas particles are moving away from the hot surface preventing deposition on the bottom substrate. The cooler top plate is not directly heated making it easier for the smaller particles to penetrate the boundary layer. Hence in the process a degree of nanoscale sieving has occurred. The smaller nanoparticles can be incorporated in a film whilst the larger aggregated ones are repelled and exit to the exhaust.

We have shown that solid nanoparticulate starting materials, provided they can be suspended/dissolved in an appropriate solvent, do make useful precursors for the formation of thin films. This process has not been termed CVD as such as no overriding chemical reaction seems to have occurred, the initial material and final material were very similar by XRD, save some possible grain growth. However some interaction and bonding has occurred between the underlying substrate and the particles as the film is adhesive. The new deposition method developed here is similar to suspension plasma spraying of nanoparticles,[26] but avoids the use of a plasma and a high velocity stream, and hence is much simpler to use and operate.

A comparison was made between the aerosol-assisted process described above and using a spin coating or evaporation technique using the same WO_3/toluene nanoparticulate suspension. The films formed by spin coating both before and after firing were nonadhesive and powdery. The SEM of the films are very similar to those formed by AAD with particles matching those seen in the AACVD experiments. However, an important difference is that these films failed the Scotch tape test, and could be wiped off with a tissue, unlike those formed in the AAD process.

Preparation of Titania Films in the Presence of Tungsten Oxide Nanoparticles

Aerosol-assisted chemical vapour deposition of anatase titania was accomplished from $[Ti(OiPr)_4]$ dissolved in toluene at a deposition temperature of 450 °C in the presence of tungsten oxide nanoparticles. The films of TiO_2 formed in the presence of WO_3 nanoparticles were generally a very pale yellow-beige – compared to the colourless or white films formed from $[Ti(OiPr)_4]$ alone. Some "rainbow-like" interference fringes could be seen in reflection at the edges of the film due to variations in thickness. The films passed the Scotch tape test and were resistant to wiping but could be scratched with a brass scalpel. They showed minimal specular haze assessed as 2%. The films showed good transmission between 50 and 60% in the visible region. The films formed both on the heated substrate and the top plate – unlike the WO_3 nanoparticle experiments where the film was only on the unheated top plate. The same microstructures and analysis were seen for both top and substrate plates.

Wide-area EDAX analysis showed that the films were made up of titanium and oxygen with just a trace of tungsten present (detectable but less than 1 atom% – and so not directly quantifiable). SEM imaging showed a plate-like morphology oriented perpendicular to the substrate of dimension ca 500 nm by 10 nm and underlying plates in a seemingly "wedding cake" structure, Figure 3. This microstructure is to the best of our knowledge unique for a titania film – and was repeatable in over five separate repeat

experiments. Indeed each particle seemed to have the self-same highly structured shape and were arranged as if in a mosaic pattern across the surface made up of a similar repeating units. High resolution SEM or spot EDAX analysis did not find any tungsten oxide particles. Previous work on titania by AACVD and APCVD on glass and indeed deposition of TiO_2 from $[Ti(OiPr)_4]$ from this work has always formed a smooth continuous film or a random island-like growth.[30] Hence as all other factors were the same the presence of the tungsten nanoparticles is the most likely cause of this unique surface architecture. Side-on SEM images allowed the determination of the film thickness and hence the growth rate of the films. It was found that the film thickness was 7–10 μm depending on the film sample analysed. The growth rate was calculated to be 3.5–10 μm per hour.

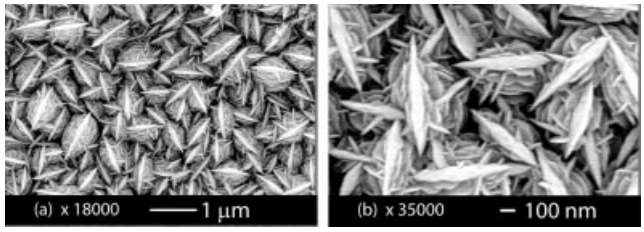

Figure 3. Scanning electron micrograph of the TiO_2 films formed at 450 °C by the aerosol-assisted deposition of $[Ti(OiPr)_4]$ in the presence of nanoparticulate WO_3: a) at 18000 times magnification; and b) at 35000 times magnification.

The thin film of TiO_2 deposited with WO_3 nanoparticles was investigated using powder X-ray diffraction, and then modelled using Rietveld refinement.[28] The pattern was found to be well modelled by the anatase phase of TiO_2 [$I4_1/amd$, a = 3.7804(3) Å, c = 9.500(2) Å], once the lattice and peak profile parameters were refined and preferred orientation taken into account (See Figure 4 and Figure 5). The preferred orientation was modelled using the March–Dollase model.[34] A good match to the recorded data was found when the 110 plane was used as the preferred plane with a March coefficient of r = 0.542(2), a measure of the sample compression/elongation due to preferred orientation. As the SEM images indicate the crystallites are plate-like (rather than rod-like) then, as the value of r is less than 1, we can conclude that the crystals are preferentially aligned so that the 110 plane is parallel to the deposition surface.[30]

Additional peaks were also found in the pattern for the part of the film that was 5 cm from the reactor inlet (marked with *asterisks* in Figure 5). These could be indexed as belonging to a cubic cell with lattice parameter a = 5.646 Å and systematic absences consistent with face-centred symmetry. These peaks were of much lower intensity than those corresponding to TiO_2, suggesting that this phase is present only in small amounts. A search of the inorganic crystal structure database was conducted to identify this phase, but no reasonable match could be found.

The Raman patterns for the titania films (recorded at multiple points across the films surface) showed the expected bands for anatase with bands at 143, 396, 515 and 612 cm^{-1}, no evidence was seen for any tungsten oxide phase at any part of the deposited film.

The titania films were very hydrophilic as formed. Typical initial water droplet contact angles were around 5–10°, this is smaller than that found for a typical titania coating formed by CVD which gave initial water contact angles of ca 30°.[32,33] This difference in contact angle can be attributed to the microstructure seen from the SEM measurements. The films exhibited photo-induced superhydrophilicity. The films were also photocatalytically active showing ready destruction of a stearic acid over-layer with both 254 and 365 nm radiation and were comparable in photodegradation ability to previously analysed sol-gel and CVD prepared titania.[35] Using 254-nm light half of the stearic acid coating was removed in 1.2 h (4×10^{12} mole-

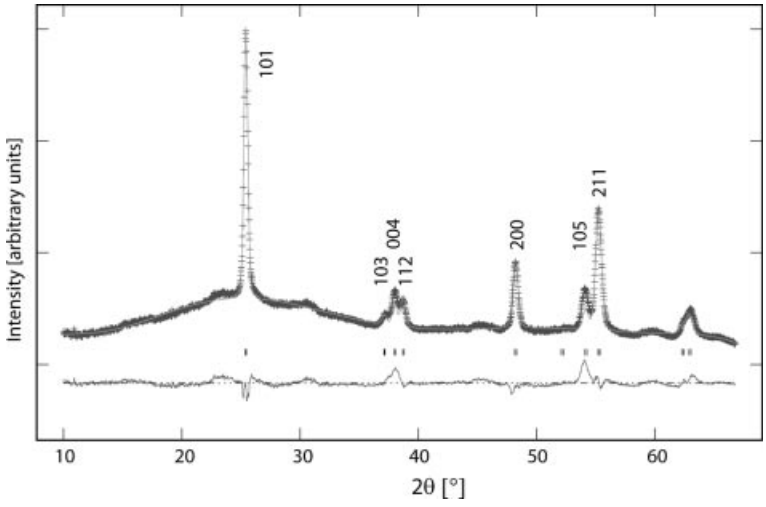

Figure 4. Rietveld refinement of TiO_2 films formed at 450 °C by the aerosol-assisted deposition of $[Ti(OiPr)_4]$ in the presence of nanoparticulate WO_3. Diffraction data shown by crosses, upper continuous line is the refined model, and lower line is the difference plot. Pattern was obtained from the surface of the glass some 2 cm away from the reactor inlet.

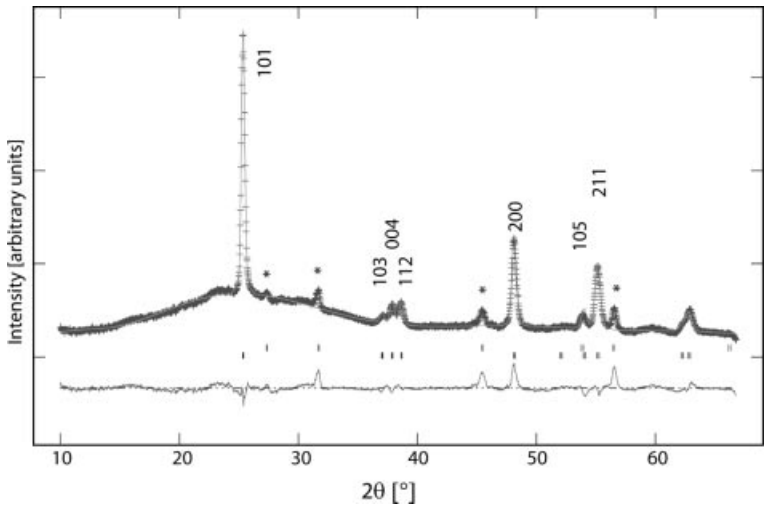

Figure 5. Rietveld refinement of TiO_2 films formed at 450 °C by the aerosol-assisted deposition of [Ti(O*i*Pr)$_4$] in the presence of nanoparticulate WO_3. Diffraction data shown by crosses, upper continuous line is the refined model, and lower line is the difference plot. The lower set of tick marks correspond to the TiO_2 main phase. The higher set of tick marks are the indexed second phase (*F* cubic, a = 5.646 Å), these peaks are also marked by asterisks. Pattern was obtained from the surface 5 cm away from the reactor inlet.

cules cm^2 min^{-1} for 254 nm) compared to 2.2 h for a comparable 365-nm source.

As a comparison to the films formed by AACVD the same WO_3 nanoparticulate-[Ti(O*i*Pr)$_4$] precursor solution was used to make sol-gel dip-coated films (Figure 6). The reason for this study was to see whether the unusual microstructure would follow in films made from the same precursor solution – but processed in a different way. By using the sol-gel process a nonadhesive, pale yellow, powdery film resulted. This was unlike those formed by AAD that adhered well to the substrate. Furthermore, the SEM of the films showed a particulate microstructure. Hence the fine structure seen in the AAD route was not in evidence and indicates the uniqueness of that approach in controlling – influencing the underlying microstructure. This microstructure gave rise to an important functional property – a very low water contact, much lower than that seen in conventional titania films formed by APCVD, AACVD or sol-gel methods. The unusual microstructure with the crenulated surface texture is most likely responsible for this low value. The ability to have very low contact angles for water is an important criteria for self-cleaning applications for example on windows. Indeed a number of commercial products (Pilkington Activ, Saint Goban Bioclean and PPG sunclean) all make use of this phenomena. The contact angles seen in this work for the structured films are lower than those reported for the commercial products – which typically have values around 10°. One counter point is that the microstructure induces more diffuse specular reflectance (haze) of around 2% compared to commercial windows that have a value of less than 0.2%.

The role of the tungsten oxide nanoparticles in engendering the unusual microstructures has not been fully elucidated in this work. The tungsten oxide obviously plays a major role because in its absence the films of titania formed are continuous and lack the self-similarity across the surface. Tungsten has been detected in the films albeit at ca 1 atom% level. This tungsten has not been seen as individual nanoparticles and spot EDAX analysis can find no evidence of localised high tungsten concentrations. It is possible that some tungsten has been incorporated in the titania lattice in the form of a solid solution- however the Raman and XRD provide no evidence for this in terms of changes in peak position or lattice parameter. The presence of a small amount of secondary phase in the XRD pattern suggests that this could be playing a structurally directing role. The phase is present at only a percent and although few peaks are seen it does match well for a cubic cell.

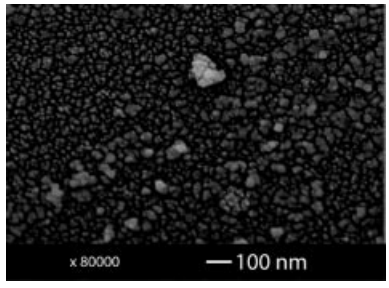

Figure 6. SEM of the WO_3–TiO_2 film formed by sol-gel dip coating followed by firing at 550 °C.

We have previously reported on the use of preformed – soluble ionic nanoparticles for the formation of composite thin films.[36] In that case gold nanoparticles were generated and then encapsulated in a titania or tungsten oxide matrix. That work is different to that reported here in that the nanoparticles were dissolved in solution rather than acting as a suspension. Further, the films generated did not have any unusual microstructures – the gold was simply embedded in the host matrix. Hence by using a commercial solid nanoparticulate powder we have shown that it is possible to make adherent thin films composed of nanoparticles, and

that the presence of these particles can affect the surface morphology of titanium dioxide. The nanoparticles used in these experiments were unlike conventional methods that use nanoparticles – where they are charged or ligand stabilized.

Conclusions

Aerosol-assisted deposition (AAD) was used to deposit WO_3 nanoparticle thin films from a solid nanoscaled precursor. This was a convenient method for applying thin films to glass as it provides reasonable growth rates (3–7 $\mu m\,h^{-1}$) and conformal coverage of the substrate. The films were adhesive and were superhydrophilic. This route shows promise for the formation of thin films of material from involatile nanoscaled solid precursor and is the antithesis of what would normally be required for thin film deposition – i.e. a molecular volatile precursor. Titania films formed in the presence of WO_3 nanoparticles form unique microstructures and exhibited two key functional properties, photocatalysis and photoinduced superhydrophilicity. The initial water contact angles of these films are considerably lower than that seen for TiO_2 films prepared in the absence of nanoparticles and is attributed to the "fractal-like" microstructure.

Experimental Section

Solid WO_3 nanoparticles and titanium tetraisopropoxide were obtained from Aldrich and used as supplied (99% purity). The pale yellow WO_3 nanoparticles (typically 0.2 g, 0.862 mmol) were sonicated by an ultrasonic bath (2 h) to aid dispersion in toluene (40 mL). This produced a pale yellow solution with some undissolved solid. This solution was used as a precursor for aerosol-assisted transport to form WO_3 films on glass. A similar concentration solution of WO_3 in toluene was used to make WO_3–TiO_2 thin films – except in that case titanium isopropoxide (0.56 g, 1.972 mmol) was added to the initial precursor solution (W: Ti molar ratio 1:2.28). It should be noted that on leaving the nanoparticulate suspension to stand for 12 h the solution became colourless and by weight seemingly all of the initial particles came out of the solution.

Three series of AACVD experiments were conducted using the following starting solutions/suspensions:

i) A suspension of WO_3 nanoparticles (0.2 g, 0.862 mmol) in toluene (40 mL) to form WO_3 thin films.

ii) [Ti(O*i*Pr)$_4$] (0.56 g, 1.972 mmol) dissolved in toluene (40 mL) to form TiO_2 films.

iii) A mixture of suspended WO_3 nanoparticles (0.2 g 0.862 mmol) and [Ti(O*i*Pr)$_4$] (0.56 g, 1.972 mmol) dissolved in toluene (40 mL) to form highly ordered microstructures

All AACVD experiments were performed on a custom built apparatus consisting of a horizontal-bed cold-wall reactor connected to an arrangement of delivery tubing, a bubbler and a humidifier – full details of the reactor have been published previously.[27]

The CVD reactor itself consisted of a silica glass substrate and supported top plate in a cylindrical quartz tube. The cylindrical quartz tube was open at both ends with each end capped by a stainless steel plate. Nitrogen gas entered the system through a brass manifold, which generated an uniform flow of gas across the width of the reactor. The uniform flow then passed between the heated glass bottom plate and the unheated glass top plate that was 5 mm above the heated surface. Thus a channel is present for the gas to flow between. The glass substrates of dimensions $150 \times 45 \times 4$ mm were heated by a graphite block that contained a Whatman cartridge heater. The glass substrates (both top plate and heated bottom plate) were supplied by Pilkington Glass and were pre-coated with a SiO_2 barrier layer. This barrier layer prevented atoms within the glass diffusing into the deposited film.

A typical deposition experiment proceeded as follows. The precursor mixture was transferred to the aerosol chamber, a customised PTFE container. A flow of nitrogen (BOC, 99.99%) was passed through the apparatus at all times. The glass substrate was cleaned using a tissue soaked in water, then with a tissue soaked with propan-2-ol. The glass was allowed to dry in air prior to it being mounted in the CVD chamber. The temperature of the glass inside of the reactor was measured by Pt–Rh thermocouples. Depositions were conducted at 400, 450 and 500 °C. Once the temperature was stabilised, an aerosol was then generated using an ultrasonic humidifier, and nitrogen gas passed through the aerosol mist (2 $L\,min^{-1}$), directing the aerosol to the CVD reactor. The aerosol passed through the brass manifold and entered the reactor between the heated substrate and the glass top-plate, placed parallel to the substrate. Any waste products exited through the exhaust. The gas flow was continued until all the precursor mix had passed through the reactor, typically taking 1 to 2 hours depending on the gas flow rate, carbon reactor temperature and solvent. The coated films on glass were cooled to room temperature in situ under a flow of N_2, and after cooling were handled and stored in air.

Spin Coating/ Evaporation Coating: Films of WO_3 and TiO_2/WO_3 were made by spin and evaporation coating of the precursor solutions mentioned above (0.2 g of WO_3 and 0.56 g of [Ti(O*i*Pr)$_4$] in toluene (40 mL). These coatings were fired in a furnace at 550 °C for 1 hour in air. The purpose of these experiments was to explore the differences in microstructure, surface adhesion and durability of the coating compared to those formed by the AACVD route.

Film Analysis: X-ray diffraction patterns were measured with a Bruker GADS using Cu-K_α radiation ($K_{\alpha 1}$ = 1.5406 Å). The system had a focussed and movable *x*-*y* stage to analyse various portions of the film. The diffractometer used glancing incident radiation (1.5°). The diffraction patterns were modelled using the Reitveld method with the GSAS suite of programmes and were compared to database standards.[25] EDAX was obtained on a Philips XL30E-SEM instrument and SEM was obtained with a JEOL 6301 instrument. UV/Vis/NIR spectra were recorded in the range 190–1100 nm using a Helios double beam instrument. Reflectance and transmission spectra were recorded between 300 and 1200 nm by a Zeiss miniature spectrometer. Reflectance measurements were standardised relative to a rhodium mirror and transmission relative to air. Raman spectra were acquired with a Renishaw Raman System 1000 using a helium-neon laser of wavelength 632.8 nm. The Raman system was calibrated against the emission lines of neon.

The photocatalytic properties of the samples were assessed by the destruction of an overlayer of a test organic stearic acid on a 3×3 cm portion of coated glass. This coated glass had been irradiated at 254 nm for 1 h prior to measurement. The stearic acid was applied by dropping 7.5 μL of a 0.4-mmol solution of stearic acid in methanol onto the glass surface which was spun at 1500 revolutions a minute during the dropping procedure. The infrared spectra

of the stearic-acid overlayer was measured over the range 2950–2800 cm^{-1}. The glass coated with stearic acid was irradiated with 365-nm radiation provided by BDH germicidal lamps (2 × 8 W). The IR spectra of the stearic acid was measured after 30 min intervals for up to 2 h and the areas of the bands that attributed to the C–H stretches were quantified.

The advancing water contact angles were determined by measuring the width of a known volume of water (1 μL) with a travelling microscope and then entering the spread into a simple trigonometric program.

Acknowledgments

Engineering and Physical Sciences Research Council (EPSRC) and Pilkington Glass are thanked for financial support. The Royal Society and Wolfson Trust are thanked for providing a merit award to IPP.

[1] *Nanoscience and Nanotechnologies*, The Royal Society and The Royal Academy of Engineering, **2004**, London.
[2] G. Schmid (Ed.), *Nanoparticles – From Theory to Applications*, John Wiley & Sons, New York.
[3] V. Subramanian, E. E. Wolf, P. V. Kamat, *J. Am. Chem. Soc.* **2004**, *126*, 4943.
[4] T. Ung, L. M. Liz-Marzan, P. Mulvaney, *Colloids Surfaces A: Physiochem. Eng. Aspects* **2002**, *202*, 119.
[5] X. Xu, M. Stevens, M. B. Cortie, *Chem. Mater.* **2004**, *16*, 2259.
[6] Z. Liu, H. Wang, H. Li, X. Wang, *App. Phys. Lett.* **1998**, *72*, 1823.
[7] T. Mokari, H. Sertchook, A. Aharoni, Y. Ebenstein, D. Avnir, U. Banin, *Chem. Mater.* **2005**, *17*, 258.
[8] K. Naoi, Y. Ohko, T. Tatsuma, *J. Am. Chem. Soc.* **2004**, *126*, 3664.
[9] C. Yang, M. Kalwei, F. Schuth, K. Chao, *App. Catal. A: Gen.* **2003**, *254*, 289.
[10] M. Lee, L. Chae, K. C. Lee, *NanoStructured Mater.* **1999**, *11*, 195.
[11] D. Lahiri, V. Subramanian, T. Shibata, E. E. Wolf, B. A. Bunker, P. V. Kamat, *J. App. Phys.* **2003**, *93*, 2575.
[12] S. Schimpf, M. Lucas, C. Mohr, U. Rodemerck, A. Bruckne, J. Radnik, H. Hofmeister, P. Claus, *Catal. Today* **2002**, *72*, 63.
[13] Y. Hida, H. Kozuka, *Thin Solid Films* **2005**, *476*, 264.
[14] T. He, Y. Ma, Y. Cao, W. Yang, J. Yao, *Phys. Chem. Chem. Phys.* **2002**, *4*, 1637.
[15] T. He, Y. Ma, Y. Cao, W. Yang, J. Yao, *J. Electroanalytical Chem.* **2001**, *514*, 129.
[16] Y. Tian, T. Tatsuma, *Chem. Commun.* **2004**, 1810.
[17] A. L. Stepanov, V. N. Popok, *Technol. Phys. Lett.* **2003**, *29*, 977–979.
[18] K. Fukumi, A. Chayahara, K. Kadono, T. Sakaguchi, Y. Horino, *J. Appl. Phys.* **1994**, *75*, 3075.
[19] E. Stathatos, P. Lianos, P. Falaras, A. Siokou, *Langmuir* **2000**, *16*, 2398.
[20] Y. Yang, J. Shi, W. Huang, S. Dai, L. Wang, *J. Mater. Sci.* **2003**, *38*, 1243.
[21] M. Epifani, C. Giannini, L. Tapfer, L. Vasanelli, *J. Am. Ceram. Soc.* **2000**, *83*, 2385.
[22] C. Bechinger, S. Herminghaus, P. Leiderer, *Thin Solid Films* **1994**, *239*, 156.
[23] C. M. Afzaal, K. Elwood, N. L. Pickett, P. O'Brien, J. Raffety, J. Waters, *J. Mater. Chem.* **2004**, *14*, 1310.
[24] G. Montavon, *High Temp. Mater. Processes* **2004**, *8*, 45.
[25] R. B. Heimann, *Adv. Ceram. Mater. Key Eng. Mater.* **1996**, *122*, 399.
[26] C. Borchers, F. Gartner, T. Stoltenhoff, H. Kreye, *J. Appl. Phys.* **2005**, *96*, 4288.
[27] I. P. Parkin, G. E. Elwin, *Chem. Vap. Dep.* **2000**, *6*, 59.
[28] C. Blackman, I. P. Parkin, *Chem. Mater.* **2005**, *17*, 1583.
[29] A. C. Larson, R. B. Van Dreele, "*General structure analysis system (GSAS)*". Los Alamos national laboratory report LAUR 86–748, **2000**.
[30] P. M. Woodward, A. W. Sleight, J. Voight, *J. Phys. Chem. Solids* **1995**, *56*, 1305.
[31] R. G. Palgrave, I. P. Parkin, *J. Mater. Chem.* **2004**, *14*, 2864; W. B. Cross, I. P. Parkin, S. A. O'Neill, *Chem. Mater.* **2003**, *15*, 2786.
[32] W. B. Cross, I. P. Parkin, *Chem. Commun.* **2003**, 1696.
[33] S. A. O'Neill, I. P. Parkin, R. J. H. Clark, A. Mills, N. Elliott, *J. Mater. Chem.* **2003**, *13*, 56.
[34] W. A. Dollase, *J. Appl. Crystallogr.* **1986**, *19*, 267.
[35] A. Mills, A. Lepre, N. Elliott, S. Bhopal, I. P. Parkin, S. A. O'Neill, *J. Photochem. Photobiol. A: Chem.* **2003**, *160*, 185.
[36] R. Palgrave, I. P. Parkin, *J. Am. Chem. Soc.* **2006**, *128*, 1587.
Received: December 19, 2006
Published Online: February 21, 2007

